Applied Catalysis B: Environmental 212 (2017) 185–192

Contents lists available at ScienceDirect

Applied Catalysis B: Environmental

journal homepage: www.elsevier.com/locate/apcatb

Efficient enantioselective degradation of the inactive (*S*)-herbicide dichlorprop on chiral molecular-imprinted TiO_2

Ya-Nan Zhang [a,1], Weiguo Dai [a,1], Yuezhong Wen [b,*], Guohua Zhao [a,*]

[a] School of Chemical Science and Engineering, Shanghai Key Lab of Chemical Assessment and Sustainability, Key Laboratory of Yangtze River Water Environment, Tongji University, Shanghai 200092, China
[b] Institute of Environmental Science, College of Environmental and Resource Sciences, Zhejiang University, Hangzhou 310058, China

ARTICLE INFO

Article history:
Received 15 February 2017
Received in revised form 14 April 2017
Accepted 24 April 2017
Available online 24 April 2017

Keywords:
Herbicide dichlorprop
(*S*)-DCPP enantiomers
Enantioselective degradation
Molecular-imprinted single-crystalline TiO_2
Anti-interference ability

ABSTRACT

The chiral compound 2-(2,4-dichlorophenoxy) propionic acid (DCPP) is a widely used herbicide; the active (*R*)-DCPP enantiomer has been reported to often be preferentially degraded, whereas the inactive (*S*)-DCPP with greater toxicity remains in the environment. In this study, we achieved efficient enantioselective recognition and controllable degradation of (*S*)-DCPP on a photoelectrocatalytic (PEC) surface by introducing a molecular imprinting technique. We fabricated an (*S*)-DCPP-molecular-imprinted single-crystalline TiO_2 (*S*-TiO_2 (SC)) photoelectrode in situ by constructing (*S*)-DCPP molecular imprinting sites on the surface of 1D single-crystalline TiO_2 nanorods. The results revealed that the *S*-TiO_2 (SC) exhibited higher PEC oxidation activity (0.500 mA/cm^2) and electrochemical surface adsorption (4.37×10^{-12} mol cm^{-2} mg) against the target (*S*)-DCPP than against the non-target (*R*)-DCPP. Additionally, the *S*-TiO_2 (SC) achieved excellent enantioselective PEC degradation of (*S*)-DCPP in both the single component and racemic systems. The *k* value of (*S*)-DCPP was 0.156 h^{-1} after 6 h, which was 2.6 times greater of (*R*)-DCPP (0.060 h^{-1}). Finally, when (*S*)-DCPP was present with 100-fold concentration of (*R*)-DCPP and five other contaminants, a greater anti-interference ability was demonstrated by *S*-TiO_2 (SC). This study highlights the need for further investigations on the enantioselective degradation of a specific enantiomer in chiral enantiomers.

1. Introduction

Chemical pesticides have played important roles in modern agriculture because of their ability to effectively control pests. However, the widespread application of pesticides has resulted in their ubiquitous occurrence in microorganisms, plants, soil, and especially in water because of their high water solubility [1–3], causing severe environmental problems [4]. Therefore, the environmental pollution control and treatment of poisonous pesticides are important and are a major concern of researchers [5].

Among the chemical pesticides, up to 30% of those currently used are chiral and consist of at least two enantiomers that usually exhibit different biological properties, toxicity and metabolism in biological systems [6–8]. These differences cause differences in microbial degradation rates [9] where one enantiomer is more persistent than others in the environment, resulting in their relative enrichment [10–15]. Faller et al. [16] determined the concentration ratio of enantiomers in the North Sea and confirmed that two α-HCH enantiomers were degraded at different rates by marine bacteria. Lewis's group [17] reported that many factors, including the fungi and microbes in the soil, affect the selective environmental behaviors of chiral pesticides. Liu et al. [18] studied the degradation of chiral cypermethrin in precipitates and revealed that the degradation of *trans*-cypermethrin was much faster than that of the *cis*-form. However, in some cases, the active component of a racemate was preferentially degraded, resulting in the relative enrichment of the other inactive enantiomer. For instance, in the case of the chiral compound 2-(2,4-dichlorophenoxy) propionic acid (DCPP) that is a widely used racemic herbicide, the active (*R*)-enantiomer was found to be preferentially degraded in seawater by marine microorganisms, whereas the (*S*)-enantiomer remained in the environment [19]. Although commercial DCPP is sold predominantly as the (*R*)-enantiomer, the active one is easily isomerized to the inactive (*S*)-enantiomer with greater toxicity and persistency [20]. Therefore, the enantioselective removal of a specific chiral enantiomer,

* Corresponding authors.
E-mail addresses: wenyuezhong@zju.edu.cn (Y. Wen), g.zhao@tongji.edu.cn (G. Zhao).
[1] These authors contributed equally to this work.

http://dx.doi.org/10.1016/j.apcatb.2017.04.062
0926-3373/

especially the inactive one, is considered to have important environmental implications.

Obtaining a single active enantiomer through chiral separation is usually difficult because it is a complex and expensive process [21,22]. The components and concentrations of residual enantiomers in the environment may differ because of the chiral asymmetry of enzymes, microorganisms, etc. Many studies have shown that enantioselectivity closely depends on environmental conditions and that results may vary substantially even for the same compound compared to previous studies [23]. For example, (*S*)-metalaxyl was preferentially degraded in sludge, whereas the (*R*)-enantiomer, with bactericidal activity, was degraded faster in soil [24]. Therefore, a simple and effective method is needed for the enantioselective recognition of a specific enantiomer in a racemate and to achieve controllable oxidative degradation to reduce environment pollution and toxicity.

The photoelectrocatalytic (PEC) oxidation method is an advanced, green and highly efficient oxidation technique that has been widely used in the degradation of environmental pollutants [25–28]. The efficient PEC oxidation process for the oxidation of pollutants into carbon dioxide and water is mainly dependent on the strong oxidizing ability of hydroxyl radicals derived from photogenerated holes. However, this process is also a limitation of the PEC method because the hydroxyl radicals cannot selectively oxidize a certain substrate in a complex system, as is the case for chiral pesticides with similar molecular structures and physicochemical properties. Because the greatest distinction between chiral pesticide enantiomers is the difference in their spatial structures, the introduction of a molecular imprinting technique (MIT) into the PEC method is proposed. Through creating specific molecular recognition sites by preparing molecularly imprinted materials, the enantioselective recognition and degradation of the target enantiomer molecule can be achieved. Although the traditional MIT method of constructing a molecularly imprinted polymer (MIP) [29–32] has obviously improved the selective capacity, MIPs are unstable and have been found to easily decompose under light irradiation. If the molecularly imprinted sites are constructed on the surfaces of inorganic metal oxide nanoparticles or nanofilms, not only the good PEC performance can be retained, but also the molecularly imprinted sites are too indistinct to provide selective recognition for target molecules [33]. Therefore, achieving an efficient imprinting effect and the enantioselective recognition of chiral enantiomers simultaneously is the main objective of the enantioselective PEC method.

In this paper, in consideration of the adverse ecological effects of the inactive (*S*)-DCPP enantiomer, we construct a new system to achieve the enantioselective recognition and controllable degradation of (*S*)-DCPP using molecular-imprinted single-crystalline TiO_2 nanorods (SC TiO_2 NRs). A simple hydrothermal method is used to construct the (*S*)-DCPP molecularly imprinted TiO_2 nanorods (*S*-TiO_2 (SC)) with (*S*)-DCPP as the template molecule. The enantioselective PEC recognition and the oxidation ability of (*S*)-DCPP in single and racemic systems are investigated. The difference in degradation kinetics and the reaction mechanism are also studied. For comparison, the (*S*)-DCPP was also imprinted onto 0 D polycrystalline TiO_2 nanorods (*S*-TiO_2 (PC)) via a liquid-phase deposition method. The enantioselective PEC degradation of the target enantiomers on *S*-TiO_2 (SC) is evaluated through analysis of the enantiomers' different adsorption effects on the surface. Our work represents a creative method for the controllable enantioselective degradation of DCPP enantiomers, providing a reasonable approach for the removal of specific chiral pesticide enantiomers in wastewater treatment.

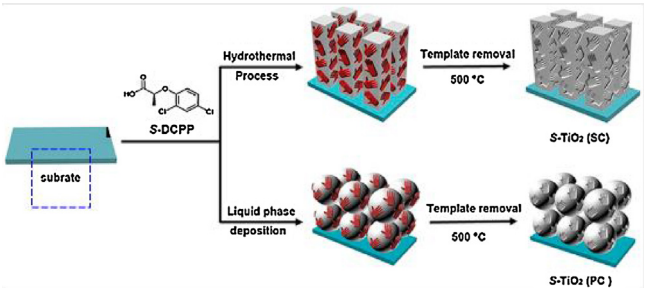

Scheme 1. Schematic of the fabrication process of the photoelectrodes.

2. Experimental section

2.1. Materials and apparatus

Na_2SO_4, titanium (IV) butoxide (99.0%), HCl, humic acid, glyphosate, omethoate, metolachlor, and atranex were of analytical grade and were used without further purification. (*S*)-Dichlorprop and (*R*)-dichlorprop with 99% purity were synthesized according to Camps' method [34]. The electrode was characterized by field-emission scanning electron microscopy (FE-SEM, Hitachi-S4800, Japan), transmission electron microscopy (TEM, JEM-2100, JEOL), X-ray diffraction (XRD, Bruker D8 Advance, Germany), and Raman spectroscopy (inVia Reflex, Renishaw, UK). Fourier transform infrared spectroscopy (FT-IR, Thermo Nicolet, Nexus, USA) was used to investigate the formation of molecular imprinting sites.

2.2. Synthesis of chiral molecularly imprinted TiO_2 photoelectrodes

FTO was cut into $1.5 \times 4.0\ cm^2$ pieces and used as the substrate electrode after being cleaned in a mixed solution of deionized water, acetone, and 2-propanol. In a typical hydrothermal synthesis (HTS), 10 mL of concentrated HCl (38%) and 10 mL of deionized water were mixed; 0.25 mL of titanium (IV) butoxide (99.0%) was then added dropwise with vigorous stirring. After stirring for 1 h, the precursor solution was transferred to a 25 mL Teflon autoclave with FTO and maintained at 150 °C for 4 h. After the reaction, the electrode was rinsed with deionized water and annealed at 500 °C for 30 min; the TiO_2 (HTS) product was thus obtained. The (*S*)-DCPP imprinted *S*-TiO_2 (*S*-TiO_2 (HTS)) and (*R*)-DCPP imprinted TiO_2 (*R*-TiO_2 (HTS)) photoelectrodes were prepared by addition of 10 μmol/L (*S*)-DCPP and (*R*)-DCPP template molecules into the precursor solution mentioned above, respectively. (*S*)-DCPP template molecules would be grown on the TiO_2 surface during the hydrothermal process. Then the template molecules were efficiently cleaned off from the surface by simple thermal treating at 500 °C for 30 min.

For comparison, a liquid-phase deposition (LPD) method was also used to prepare the (*S*)-DCPP- and (*R*)-DCPP-imprinted TiO_2 (*S*-TiO_2 (LPD) and *R*-TiO_2 (LPD), respectively). H_3BO_3 (0.1546 g) and 0.4948 g $(NH_4)_2TiF_6$ were dissolved in 25 mL of deionized water and then 10 μmol/L of the (*S*)-DCPP or (*R*)-DCPP template molecule was added. Finally, the *S*-TiO_2 (LPD) and *R*-TiO_2 (LPD) photoelectrodes were obtained after put FTO into the mixed solution with LPD process for 6 h. The template molecules were removed for heating at 500 °C for 30 min. The fabrication procedure for the two types of molecularly imprinted TiO_2 photoelectrodes is shown in Scheme 1.

2.3. PEC measurements

The photoelectrochemical performance was assessed in a three electrode cell system of a CHI 660c electrochemical workstation

(CH Instrument, USA). The prepared photoelectrodes were used as working electrode, a platinum foil was the counter electrode\\, and a saturated calomel electrode (SCE) was the reference electrode. A 150W LA-410UV-3 lamp (Hayashi, Japan) served as the visible-light source (wavelength of 420–800 nm). The amperometric i-t method was employed to monitor the PEC current at a constant potential of 0.6 V (vs SCE) in 0.1 mol/L Na_2SO_4 solution, and the working electrode was kept 1 cm away from the lamp center. The electrochemical adsorption performance of prepared photoelectrodes were carried by chronocoulometry method. And the photoelectrodes was dipped in the solution for 20 min before measured.

2.4. PEC degradation of DCPP

The PEC degradation was performed in a quartz tubular reactor equipped with a magnetic stirrer and a jacketed cooler to maintain a constant temperature (25 °C). A 300 W Xe high-pressure short-arc xenon lamp (PLS-SXE300, PerfectLight Technology Co. Ltd., Beijing) was used as the light source, providing a luminous intensity of 100 mW cm^{-2}. A 100 mL sample of 50 mg/L DCPP in 0.1 mol/L Na_2SO_4 was degraded at a bias of +0.9 V (vs. SCE) in the cell. The concentration of (*S*)-DCPP and (*R*)-DCPP were determined by the sensing analysis method. The intermediate products from the photoelectrocatalytic degradation were identified by GC–MS analysis (6890N Network GC system with a 5973 network mass selective detector). Typical ESI conditions were as follows: initial temperature 60 °C for 3 min, heating at a rate of 30 °C/min to 300 °C for 10 min. The injector port temperature was 250 °C. Helium was used as the carrier gas (1.5 mL/min). The *m*/*z* ratios are given only for the most significant peaks.

3. Results and discussion

3.1. Enhanced oxidation difference between (S)- and (R)-DCPP enantiomers on single-crystalline imprinted TiO_2 surface

Fig. 1 shows the PEC oxidation current density of the two kinds of photoelectrodes by the hydrothermal and LPD methods. As evident in Fig. 1A and B, the photocurrent increments of (*S*)-DCPP (ΔI_S) and (*R*)-DCPP (ΔI_R) were 0.120 and 0.110 mA/cm^2 on the pure TiO_2 (HTS), whereas they were 0.085 and 0.080 mA/cm^2 on the pure TiO_2 (LPD). These results reveal that the photocurrent responses of (*S*)-DCPP and (*R*)-DCPP were nearly the same, whatever on the pure TiO_2 (HTS) or TiO_2 (LPD). However, the big difference of oxidation ability for the DCPP enantiomers exited between the two kinds of photoelectrodes, while the ΔI_S (0.12 mA/cm^2) and ΔI_R (0.110 mA/cm^2) on TiO_2 (HTS) were approximately 1.4 times greater than those of TiO_2 (LPD). After the (*S*)-DCPP molecular imprinting (MI) sites were constructed on the photoelectrode surface (Fig. 1C and D), the ΔI_S and ΔI_R were 0.500 and 0.120 mA/cm^2 on the *S*-TiO_2 (HTS) and were 0.122 and 0.078 mA/cm^2 on the *S*-TiO_2 (LPD). Both ΔI_S values were much higher than the ΔI_R values, suggesting that the introduction of the MI sites greatly increased the PEC oxidation response of the target enantiomer compared to that of the non-target enantiomer. However, the ΔI_S value was 4.2 times of ΔI_R on the *S*-TiO_2 (HTS), which indicated the obvious enhancement of the PEC oxidation ability of the target enantiomer, whereas the ΔI_S value was only 1.56 times the ΔI_R value on the *S*-TiO_2 (LPD).

To analyze the differences between photoelectrodes, we characterized the morphology and crystal structure of *S*-TiO_2 (HTS) and *S*-TiO_2 (LPD) in detail (Fig. 2). The SEM and TEM images in Fig. 2D and 2E show that the structure of *S*-TiO_2 (LPD) comprises unordered, stacked zero-dimensional nanoparticles approximately 100 nm in diameter. The morphology of *S*-TiO_2 (HTS) in Fig. 2A and B shows one-dimensional, vertically aligned nanorods with well-controlled tetragonal prism structure of TiO_2 (HTS). The diameter and the length of the nanorods were 80 nm and 1 μm, respectively. In addition, a comparison of the SEM micrographs of TiO_2 (HTS) and TiO_2 (LPD) before and after constructed the MI (Fig. S1) revealed that the presence of MI sites on the surface could not influence the structure of photoelectrodes. On the basis of these results, we realized that the major distinction between the morphologies of two kinds of photoelectrodes was the critical factor affecting the PEC oxidation ability. In contrast with nanoparticles, the vertically aligned nanorods structure was more favorable for the transfer of electrons that result in efficient separation of the photogenerated electron and holes. The selected-area electron diffraction (SAED) pattern (Fig. 2F) confirms that the crystal structure of *S*-TiO_2 (LPD) was a polycrystalline structure. On the contrary, SAED pattern of *S*-TiO_2 (HTS) (Fig. 2C) reveals the structure of nanorods was an excellent single crystalline. And the lattice fringes (inset of Fig. 2B) with a spacing of 0.32 nm corresponds to the (110) facet of rutile TiO_2 [35]. Consequentially, the distinction of the crystal structure between the two types of photoelectrodes is worth attention.

As previously mentioned, the introduction of MI sites greatly increased the PEC oxidation response of the target enantiomer. This increase was mainly due to the shape-selective adsorption of the target molecules on imprinted sites. Therefore, the crystal structure of photoelectrode surface strongly determined the quality and expression of the MI sites and was the critical factor for PEC recognition of the target enantiomers. In contrast with PC structure, the SC structure was non-defective and favored the steric stability and high-quality expression of the MI sites constructed on the surface. The clear MI sites provided the shape-selective adsorption and recognition of the target template molecules.

To further clarify the recognition of the target molecules on photoelectrodes, the imprint factor, expressed as $F_{imprint}$, was defined as the ratio between the photocurrent increment caused by the target (*S*)-DCPP enantiomer and the non-target (*R*)-DCPP enantiomer [36].

$$F_{imprint} = \frac{I_{(S)\text{-DCPP}} - I_{S,blank}}{I_{(R)\text{-DCPP}} - I_{R,blank}} = \frac{\Delta I_S}{\Delta I_R} \quad (1)$$

where ΔI_S and ΔI_R are the photocurrent increase of the target (*S*)-DCPP enantiomer and the (*R*)-DCPP enantiomer obtained on the photoelectrodes' surface, respectively. The photocurrent density and $F_{imprint}$ values are listed in Table S1. Larger values of $F_{imprint}$ (>1) indicate more preferential PEC oxidation of the target enantiomer on the photoelectrodes. The $F_{imprint}$ of *S*-TiO_2 (SC) was 4.17, which was 2.7 times greater than that of *S*-TiO_2 (PC), suggesting a better imprinting effect on the *S*-TiO_2 (SC) surface.

The construction of the MI sites of (*S*)-DCPP on TiO_2 (SC) surface was confirmed by FT-IR spectroscopy (Fig. 2G). Compared with the pure TiO_2 (SC) (curve a), new peaks at 1598 cm^{-1}, 1510 cm^{-1} and 1751 cm^{-1} assigned to the aromatic ring framework vibrations and carbonyl stretching band of the carbonyl group were observed in the spectra of *S*-TiO_2 (SC) with (*S*)-DCPP template molecules (curve b). The peak at 1177 cm^{-1} corresponding to the aromatic ring and the peaks at 827 cm^{-1} and 1421 cm^{-1} corresponding to the C—H and CH_3 bending modes, were also clearly observed, respectively [37]. After template removal, only the peaks identical to pure TiO_2 could be found (curve c). However, the characteristic peaks of (*S*)-DCPP template molecules were observed again after rebinding the (*S*)-DCPP template on the surface (curve d), indicating the specific adsorption of MIs to the target (*S*)-DCPP molecules [35]. These results confirmed that the clear MIs of surface could be kept repetitively by repeated removal of the templates, implying the good recyclability of *S*-TiO_2 (SC) photoelectrode. The XRD and Raman spectra (Fig. 2H and I) further confirmed that the properties of *S*-TiO_2 (SC) remained consistent compared to those of pure TiO_2 (SC).

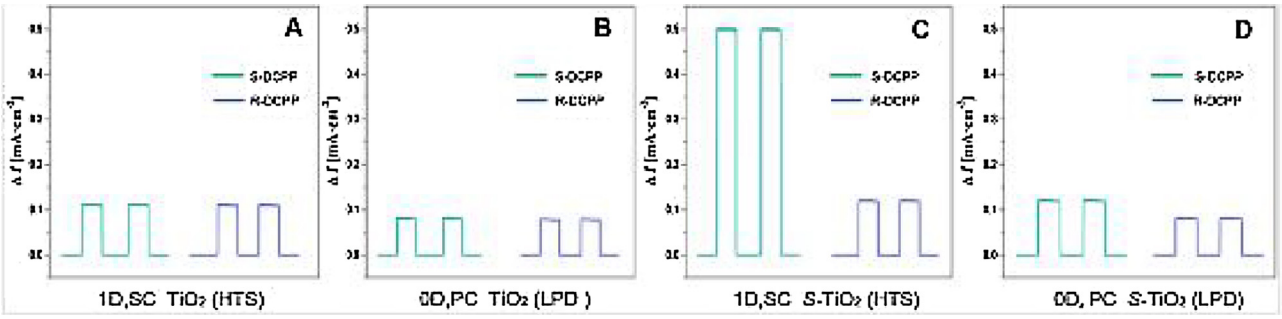

Fig. 1. PEC oxidation difference of the DCPP enantiomer on different photoelectrodes (A) 1D, SC TiO_2 (HTS), (B) 0D, PC TiO_2 (LPD), (C) 1D, SC *S*-TiO_2 (HTS), and (D) 1D, SC *S*-TiO_2 (LPD).

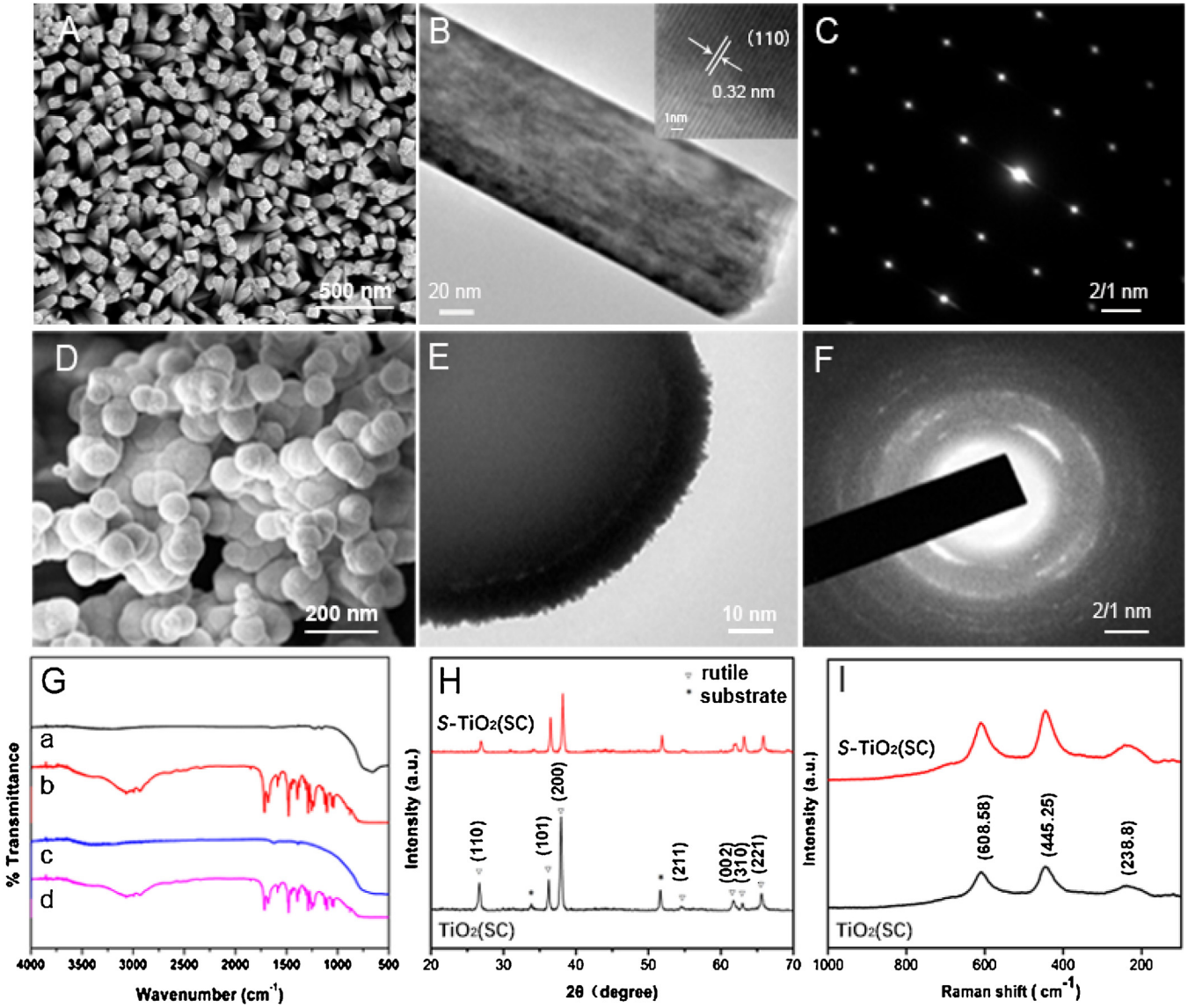

Fig. 2. (A), (D) FE-SEM images, (B), (E) TEM images, (insets: the corresponding HRTEM images), and (C), (F) SAED patterns of *S*-TiO_2 (HTS) and *S*-TiO_2 (LPD), respectively. (G) FTIR spectra of *S*-TiO_2 (SC): pure TiO_2 (SC) (a), with (b), without (c) and rebound (d) of (*S*)-DCPP template, (H) XRD, and (I) Raman spectra of TiO_2 (SC) and *S*-TiO_2 (SC).

The PEC recognition ability of the imprinted photoelectrodes for target enantiomer mainly arose from the MI sites on the surface. In contrast with the non-target enantiomer, the target enantiomer with the same spatial configuration of the MI sites was preferentially adsorbed onto the photoelectrode surface, resulting in a high concentration enrichment, and then was quickly PEC oxidized. Therefore, the electrochemical surface adsorption capacity of photoelectrodes for the target enantiomer determined by the chronocoulometry method was an efficient method to evaluate the effect of MI sites. As evident in Fig. 3A, the electrochemical adsorption of the target (*S*)-DCPP enantiomer is less than that of the non-target enantiomer (*R*)-DCPP on the TiO_2 (SC) without MI

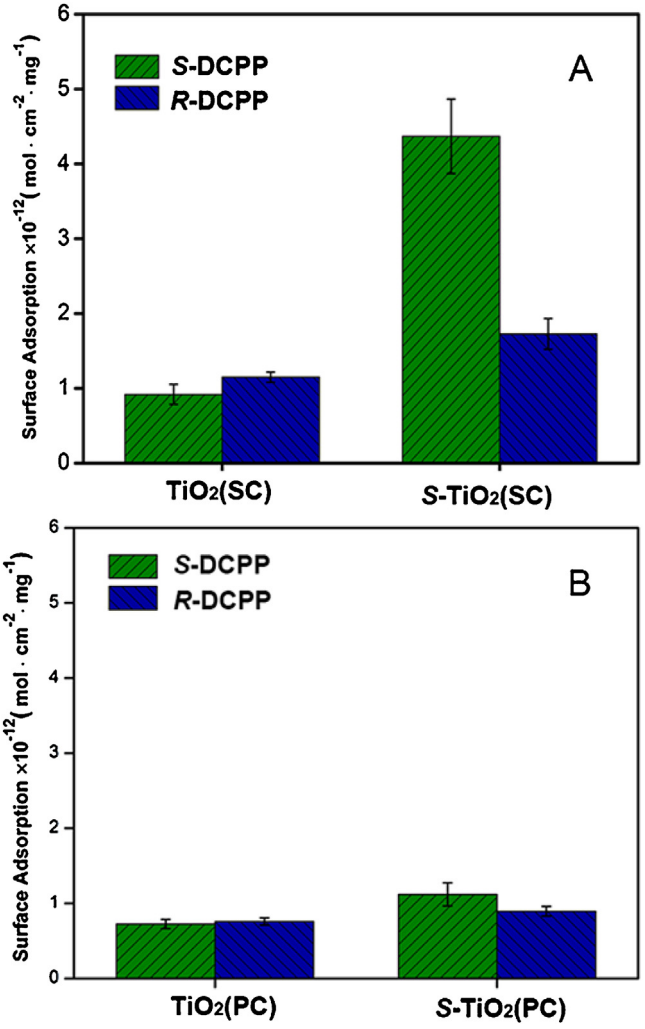

Fig. 3. Electrochemical surface adsorption performance of different photoelectrodes toward the DCPP enantiomers (A) TiO_2 (SC) and *S*-TiO_2 (SC), (B) TiO_2 (PC) and *S*-TiO_2 (PC).

sites. The same behavior was also observed in the case of TiO_2 (PC) (Fig. 3B). However, the electrochemical adsorption of (*S*)-DCPP was calculated to be 4.37×10^{-12} mol cm^{-2} mg, which is approximately 4.8-fold greater than that of (*R*)-DCPP (0.92×10^{-12}) on *S*-TiO_2 (SC) surface. Otherwise, only a small difference was observed on the *S*-TiO_2 (PC) surface. This results further demonstrates that, compared with TiO_2 (PC), the TiO_2 (SC) exhibits much better expression of MI sites on the surface because of its 1D aligned nanorod structure and non-defective single-crystal structure.

3.2. Enantioselective degradation and oxidation kinetics of (S)-DCPP

The *S*-TiO_2 (SC) photoelectrode was further applied in the degradation of DCPP enantiomers, and the oxidation kinetics were also studied. The concentration variations of (*S*)-DCPP and (*R*)-DCPP during the degradation process were determined by the sensing analysis method [38]. The concentrations of (*S*)-DCPP and (*R*)-DCPP were determined by measuring the photocurrent densities on the imprinted *S*-TiO_2 (SC) and *R*-TiO_2 (SC), respectively, when the photocurrent density and concentration exhibited a linear relationship. As shown in Fig. S2, the linear fitting equation of (*S*)-DCPP obtained for the *S*-TiO_2 (SC) was $I_{(S)\text{-DCPP}} = 2.217 \times 10^{-5}\ C + 0.00196$ (*C*: mg/L, *I*: A cm^{-2}), with a correlation coefficient of 0.9988. Additionally, the linear fitting equation of (*R*)-DCPP on *R*-TiO_2 (SC) was $I_{\text{R-DCPP}} = 2.188 \times 10^{-5}\ C + 0.00193$ (*C*: mg/L, *I*: A cm^{-2}), with a correlation coefficient of 0.9989. Therefore, the constructed *S*-TiO_2 (SC) and the *R*-TiO_2 (SC) photoelectrodes could be considered as excellent photoelectric sensors for the respective target enantiomers.

When the system contained only one enantiomer (Fig. 4A), it was only (*S*)-DCPP or (*R*)-DCPP with an initial concentration of 50 mg/L. The removal ratio and the relevant rate constants (k) of (*S*)-DCPP obtained for the corresponding imprinted *S*-TiO_2 (SC) photoelectrode were 90.9% and 0.180 h^{-1} respectively, which are similar to those of (*R*)-DCPP on *R*-TiO_2 (SC) (90% and 0.171 h^{-1}, respectively). All the degradation processes followed pseudo-first-order kinetics. The results suggested that no obvious difference of PEC oxidation ability for the target enantiomers between *S*-TiO_2 (SC) and *R*-TiO_2 (SC) photoelectrode. However, when (*R*)-DCPP was PEC-degraded by *S*-TiO_2 (SC) after 6 h, the k was calculated as 0.101 h^{-1}, which is only half of the k for (*S*)-DCPP. This result confirms that the *S*-TiO_2 (SC) photoelectrode showed obviously higher enantioselective degradation activity for target (*S*)-DCPP enantiomer than non-target (*R*)-DCPP.

When the system was racemic, containing both the (*S*)-DCPP and the (*R*)-DCPP enantiomers with an initial concentration of 50 ppm (Fig. 4B), the degradation of (*S*)-DCPP and (*R*)-DCPP on *S*-TiO_2 (SC) also followed pseudo-first-order kinetics. After 6 h, the k value of (*S*)-DCPP on the *S*-TiO_2 (SC) was 0.156 h^{-1} and the relative removal ratio was 89.2%, which were 2.6 times and 1.5 times greater than those for (*R*)-DCPP (0.060 h^{-1}, 59.1%), respectively. A selectivity factor, $F_{\text{selectivity}}$ [38,39] was defined to evaluate the enantioselective PEC oxidation ability of photoelectrodes and the data are listed in Table S3.

$$F_{selectivity} = \frac{k_{S\text{-DCPP}}}{k_{R\text{-DCPP}}} \quad (2)$$

Compared with the $F_{\text{selectivity}}$ (1.78) in the single-enantiomer system, the larger $F_{\text{selectivity}}$ (2.60) obtained in the racemic system suggests that the oxidation of (*R*)-DCPP was inhibited when a more favorable oxidation of (*S*)-DCPP occurred. This result further demonstrates that the *S*-TiO_2 (SC) photoelectrode showed great enantioselective PEC degradation of target (*S*)-DCPP enantiomer in both single-enantiomer system and racemic system. To evaluate the stablility of photoelectrodes, a recycling experiment of PEC degradation of target (*S*)-DCPPs over the *S*-TiO_2 (SC) in both single-component and racemic system were investigated. It can be seen from Fig. 4C, the removal ratio of (*S*)-DCPPs maintained at nearly constant level even after three consecutive runs. Finally, the removal ratio still remained as 90.46% in single-component system and 89% in racemic system after the third run. Additionally, the turn-over number (TON) is usually used to evaluate the catalytic activity of each active site. And the relative TON values were calculated as 1.18 after three cycles in single-component system by using the formula as follows [40,41].

$$\text{Turnover number (TON)} = \frac{Total\ moles\ of\ degraded\,(S) - DCPP}{Moles\ of\ used\ catalyst} \quad (3)$$

This results further implied that the *S*-TiO_2 (SC) photoelectrode could be used repetitively and shows a good stability and perspective of actual application. Simultaneously, the morphologies of used *S*-TiO_2 (SC) and *S*-TiO_2 (PC) after 18 h degradation was examined by SEM, which was employed to determine the structural stability of samples. As shown in Fig. S3, after comparing with as-prepared *S*-TiO_2 (SC) and *S*-TiO_2 (PC) (Fig. S3A and C), the morphologies of used samples were not obviously influenced that the structure of nanorods and nanoparticles still kept well (Fig. S3B and D), suggesting the good structure stability of photoelectrodes". Otherwise, the loading amount of TiO_2 (SC) of as-prepared and used sample were measured as 4.0 mg and 3.9 mg respectively. This is precisely indi-

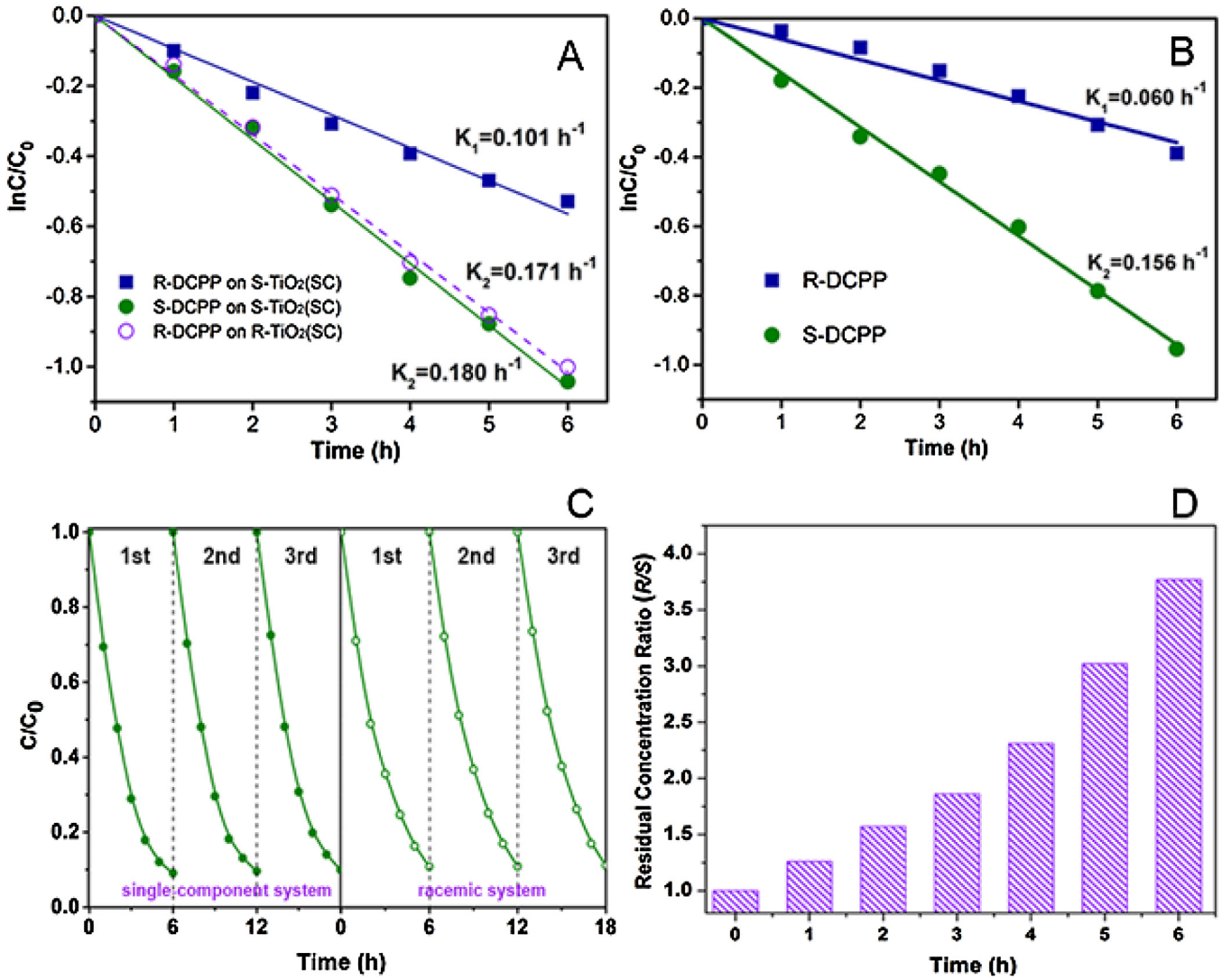

Fig. 4. PEC degradation kinetics of the DCPP enantiomers in (A) single-component system and (B) racemic system; (C) Stability of *S*-TiO_2 (SC) in PEC degradation (*S*)-DCPPs in single-component and racemic system, respectively; (D) the residual concentration ratio of the DCPP enantiomers in the racemic system.

cate the characteristics of photoelectrodes that the catalyst grown on the substrate could be used repetitively.

The difference in PEC degradation between the target (*S*)-DCPP and non-target (*R*)-DCPP enantiomers was also studied by comparing their residual concentrations in solution during the degradation process (Fig. 4D). At the beginning of degradation, the concentration ratio of (*S*)-DCPP and (*R*)-DCPP was 1:1. When the degradation time was increased from 0 to 6 h, the residual concentration ratio of (*R*)-DCPP and (*S*)-DCPP gradually increased from 1 to 3.75. The lower concentration of (*S*)-DCPP remaining in solution reveals that (*S*)-DCPP was preferentially degraded in the system in contrast to (*R*)-DCPP. Through preliminary exploration of the transformation products during the PEC degradation of (*S*)-DCPP and (*R*)-DCPP on *S*-TiO_2 (SC), we observed several similar types of intermediate products, including 2,4-dichlorophenol, chlorohydroquinone, 2-chloro-1,4-benzoquinone and oxalic acid, in both processes (Table S4). Because the degradation pathway between the (*S*)-DCPP and (*R*)-DCPP enantiomers on *S*-TiO_2 (SC) shows the similarity, the high enantioselectivity of (*S*)-DCPP was further confirmed to be mainly dependent on the preferential adsorption of target enantiomer which derived from the MI sites on imprinted photoelectrode surface.

Given that the enantioselectivity was strongly dependent on environmental factors, the PEC recognition for (*S*)-DCPP in a complex system was thoroughly studied. The (*R*)-DCPP enantiomer and other five pesticide contaminants were chosen as the interfering substances. The photocurrent increase induced by the addition of the interfering substance was used to evaluate the interference effect of interfering substance. A PEC interfering factor, $F_{\text{interference}}$, reflecting the anti-interference ability of *S*-TiO_2 (SC) was defined as follows:

$$F_{\text{interference}} = \frac{I_{\text{mix}} - I_{(S)\text{-DCPP}}}{I_{(S)\text{-DCPP}} - I_{\text{blank}}} \times 100\% \quad (4)$$

where $I_{(S)\text{-DCPP}}$ and I_{mix} are the photocurrent responses of target (*S*)-DCPP on the *S*-TiO_2 (SC) photoelectrode before and after addition of the interfering substances, respectively, I_{blank} is the photocurrent response obtained in the blank solution (0.1 mol/L Na_2SO_4), a nd $I_{\text{mix}}-I_{S\text{-DCRR}}$ is the only increase of photocurrent caused by interfering substance. A larger value of $S_{\text{interference}}$ indicates greater interference of the non-target.

As shown in Fig. 5A, to a constant concentration (25 mg/L) of (*S*)-DCPP, 1, 2, 5, 10, and 20-fold concentrations of (*R*)-DCPP were added into the system. When the concentration ratio of (*S*)-DCPP and (*R*)-DCPP was 1:1, the value of $F_{\text{interference}}$ was only 6.0%. Although

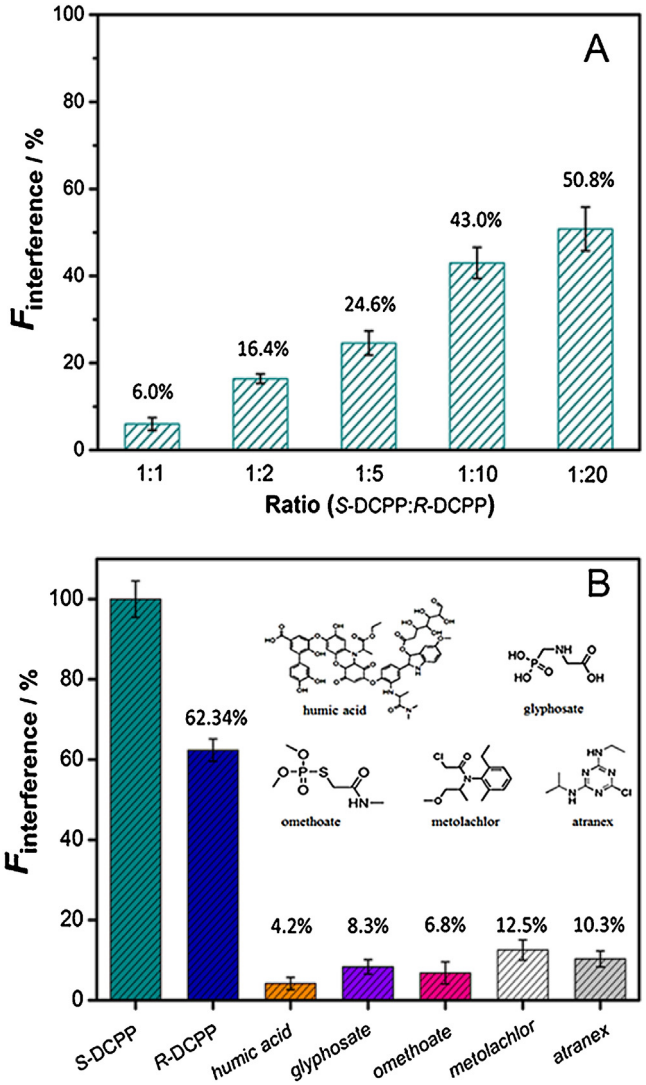

Fig. 5. (A) The anti-interference ability of *S*-TiO_2 (SC) in the racemic system with different concentration proportions of (*R*)-DCPP and (B) in the coexistent system with a 100-fold concentration of *S*-TiO_2 (SC), (*R*)-DCPP, humic acid, glyphosate, omethoate, metolachlor and atranex.

the contribution of the photocurrent increased with increase of (*R*)-DCPP concentration, the $F_{interference}$ was maintained at 50.8% even after adding the 20-fold concentration of (*R*)-DCPP. In fact, various complex pesticide pollutants coexist in the actual water environment with the DCPP enantiomers. To further evaluate the anti-interference ability of the *S*-TiO_2 (SC) photoelectrode, five pesticides—humic acid, glyphosate, omethoate, metolachlor and atranex—were chosen as the interfering substances. At a constant concentration (25 mg/L) of (*S*)-DCPP, a 100-fold concentration of a single interfering substance was individually added to the system (Fig. 5B) and all of the related I_{blank}, $I_{S\text{-}DCRR}$, I_{mix}, and $F_{interference}$ values are listed in Table S2. When (*S*)-DCPP was present with a 100-fold concentration of humic acid, glyphosate and omethoate, the $F_{interference}$ values were calculated as only 4.2%, 6.8% and 8.3%, respectively. When 100-fold concentrations of metolachlor and atranex were added into the system, the $F_{interference}$ values increased but still remained at 12.5% and 10.3% respectively. Consequently, the maximum $F_{interference}$ value of 62.3% was observed in the system containing a 100-fold concentration of (*R*)-DCPP that is the reciprocal chiral enantiomer of (*S*)-DCPP, causing the greatest interference. This result confirms that *S*-TiO_2 (SC) possessed an excellent anti-interference ability of interfering substances and high enantioselective PEC recognition of (*S*)-DCPP both in a racemic system and in a complex system containing interfering substances.

4. Conclusion

In this work, we developed an efficient method to achieve the enantioselective recognition and controllable degradation of the target (*S*)-DCPP enantiomer based on the molecular-imprinted single-crystalline TiO_2 (*S*-TiO_2 (SC)) photoelectrode surface. The result shows that the *S*-TiO_2 (SC) photoelectrode exhibits a greater chiral selective recognition ability and electrochemical adsorption of (*S*)-DCPP with $F_{imprint}$ of 4.17, while it was only 1.55 on the polycrystalline *S*-TiO_2 (PC). And the *S*-TiO_2 (SC) photoelectrode shows great enantioselective PEC degradation of the target (*S*)-DCPP enantiomer in both single-enantiomer system and racemic system.

Author contributions

The manuscript was written through contribution of all authors. All authors have given approval to the final version of the manuscript.

Acknowledgments

This work was supported by the National Natural Science Foundations of China (NSFC, No. 21537003, 21477085, 21677124 and 51208369), The 2016 Yangtze River Water Environment Key Laboratory of the Ministry of Education (YRWEF201603).

Appendix A. Supplementary data

Supplementary data associated with this article can be found, in the online version, at http://dx.doi.org/10.1016/j.apcatb.2017.04.062.

Supplementary data associated with this article can be found in the online version. Three figures (Fig. S1–S3), and 4 tables (Table S1–S4).

References

[1] E. Brillas, P.-L. Cabot, R.M. Rodriguez, App. Catal. B 51 (2004) 117–127.
[2] W. Riah, K. Laval, E. Laroche-Ajzenberg, C. Mougin, X. Latour, I. Trinsoutrot-Gattin, Environ. Chem. Lett. 12 (2014) 257–273.
[3] T. Debenest, J. Silvestre, M. Coste, E. Pinelli, Contam. Toxicol. 203 (2010) 87–103.
[4] R.M. Gonzálezrodríguez, R. Rial-Otero, B. Cancho-Grande, C. Gonzalez-Barreiro, J. Simal-Gandara, Crit. Rev. Food Sci. Nutr. 51 (2011) 99–114.
[5] H.R. Kohler, R. Triebskorn, Science 341 (2013) 759–765.
[6] Y.Z. Wen, Y.L. Yuan, H. Chen, D.M. Xu, K.D. Lin, W.P. Liu, Environ. Sci. Technol. 44 (2010) 4981–4987.
[7] A.W. Garrison, J. Gan, W.P. Liu, American Chemical Society: Washington, D.C. (2011).
[8] T. Parween, S. Jan, S. Mahmooduzzafar, T. Fatma, Z.H. Siddiqui, Crit. Rev. Food Sci. Nutr. 56 (2016) 160–179.
[9] T. Katagi, J. Pestic. Sci. 37 (2012) 1–14.
[10] J. George, Y. Shukla, J. Proteomics 74 (2011) 2713–2722.
[11] F. Vinson, M. Merhi, I. Baldi, H. Raynal, L. Gamet-Payrastre, Occup. Environ. Med. 68 (2011) 694–702.
[12] M.P. Gatto, M. Fioretti, G. Fabrizi, M. Gherardi, E. Strafella, L. Santarelli, Neurotoxicology 42 (2014) 24–32.
[13] A. Mokarizadeh, M.R. Faryabi, M.A. Rezvanfar, M. Abdollahi, Toxicol. Mech. Methods 25 (2015) 258–278.
[14] J. Ye, M.R. Zhao, L.L. Niu, W.P. Liu, Chem. Res. Toxicol. 28 (2015) 325–338.
[15] A. Lukaszewicz-Hussain, Med. Pract. 62 (2011) 543–550.
[16] J. Faller, H. Huehnerfuss, W.A. Koenig, R. Krebber, P. Ludwig, Environ. Sci. Technol. 25 (1991) 676–678.
[17] P. Ludwig, W. Gunkel, H. Hühnerfuss, Chemosphere 24 (1992) 1423–1429.
[18] W.P. Liu, J.J. Gan, S.J. Le, I. Werner, J. Agric. Food Chem. 52 (2004) 6233–6238.
[19] W. Garrison, Green. Chem. 6 (2004) 77–78.
[20] A.W. Garrison, P. Schmitt, D. Martens, A. Kettrup, Environ. Sci. Technol. 30 (1996) 2449–2455.

[21] J.L. Jarman, W.J. Jones, L.A. Howell, A.W. Garrison, J. Agric. Food. Chem. 53 (2005) 6175–6182.
[22] E. Gavioli, N.M. Maier, C. Minguillón, W. Lindner, Anal. Chem. 76 (2004) 5837–5848.
[23] D.L. Lewis, A.W. Garrison, K.E. Wommack, A. Whittemore, P. Steudler, J. Melillo, Nature 401 (1999) 898–901.
[24] M.D. Mueller, H.-R. Buser, Environ. Sci. Technol. 29 (1995) 2031–2037.
[25] S. Dosta, M. Robotti, S.G.- Segura, E. Brillas, I.G. Cano, App. Catal. B 189 (2016) 51–159.
[26] C. Guo, M. Ge, L. Liu, G. Gao, Y. Feng, Y. Wang, Environ. Sci. Technol. 44 (2010) 419–425.
[27] L. Liu, H. Liu, Y.-P. Zhao, Y. Wang, Y. Duan, G. Gao, M. Ge, W. Chen, Environ. Sci. Technol. 42 (2008) 2342–2348.
[28] Y. Ohko, K.-i. Iuchi, C. Niwa, T. Tatsuma, T. Nakashima, T. Iguchi, Y. Kubota, A. Fujishima, Environ. Sci. Technol. 36 (2002) 4175–4181.
[29] F. Deng, Y. Li, X. Luo, L. Yang, X. Tu, Colloids Surf. A 395 (2012) 183–189.
[30] A. Zander, P. Findlay, T. Renner, B. Sellergren, A. Swletlow, Anal. Chem. 70 (1998) 3304–3314.
[31] X. Shen, L. Zhu, G. Liu, H. Yu, H. Tang, Environ. Sci. Technol. 42 (2008) 1687–1692.
[32] P. Liu, W. Li, J. Zhang, J. Phys. Chem. C 113 (2009) 14279–14284.
[33] D. Sharabi, Y. Paz, App. Catal. B 95 (2010) 169–178.
[34] P. Camps, F. Perez, N. Soldevilla, Tetrahedron: Asymmetry 9 (1998) 2065–2079.
[35] H.J. Shi, J.Z. Zhao, Y.L. Wang, G.H. Zhao, Biosens. Bioelectron. 81 (2016) 503–509.
[36] Y.N. Zhang, F.Q. Nong, H.J. Shi, C.N. Chai, X.F. Huang, G.H. Zhao, Electron. Commun. 33 (2013) 5–9.
[37] Y.Z. Wen, H. Chen, C.S. Shen, M.R. Zhao, W.P. Liu, Environ. Sci. Technol. 45 (2011) 4778–4784.
[38] C. Chen, H.J. Shi, G.H. Zhao, J. Phys. Chem. C 118 (2014) 12041–12049.
[39] S.N. Chai, G.H. Zhao, Y.N. Zhang, Y.J. Wang, F.Q. Nong, M.F. Li, D.M. Li, Environ. Sci. Technol. 46 (2012) 10182–10190.
[40] C. Costentin, S. Drouet, M. Robert, J.M. Saveant, J. Am. Chem. Soc. 13 (2012) 19949–19950.
[41] Katherine Koh, M. Jeon, D.M. Chevrier, P. Zhang, C.W. Yoon, App. Catal. B 203 (2017) 820–828.